Microfluid Nanofluid (2014) 16:879–886
DOI 10.1007/s10404-013-1317-3

RESEARCH PAPER

Automating fluid delivery in a capillary microfluidic device using low-voltage electrowetting valves

Fei He · Sam R. Nugen

Received: 20 June 2013 / Accepted: 20 December 2013 / Published online: 3 January 2014

Abstract A multilayer capillary polymeric microfluidic device integrated with three normally closed electrowetting valves for timed fluidic delivery was developed. The microfluidic channel consisted two flexible layers of poly (ethylene terephthalate) bonded by a pressure-sensitive adhesive spacer tape. Channels were patterned in the spacer tape using laser ablation. Each valve contained two inkjet-printed silver electrodes in series. Capillary flow within the microchannel was stopped at the second electrode which was modified with a hydrophobic monolayer (valve closed). When a potential was applied across the electrodes, the hydrophobic monolayer became hydrophilic and allowed flow to continue (valve opened). The relationship between the actuation voltage, the actuation time, and the distance between two electrodes was performed using a microfluidic chip containing a single microchannel design. The results showed that a low voltage (4.5 V) was able to open the valve within 1 s when the distance between two electrodes was 1 mm. Increased voltages were needed to open the valves when the distance between two electrodes was increased. Additionally, the actuation time required to open the valve increased when voltage was decreased. A multichannel device was fabricated to demonstrate timed fluid delivery between three solutions. Our electrowetting valve system was fabricated using low-cost materials and techniques, can be actuated by a battery, and can be integrated into portable microfluidic devices suitable for point-of-care analysis in resource-limited settings.

Keywords Flexible microfluidics · Electrowetting valve · Inkjet printing · Lab-on-a-chip · Self-assembled monolayer

1 Introduction

Microfluidics and the miniaturization of biosensors have gained increased interest as analytical tools for medical diagnostics (Rivet et al. 2011), drug delivery, and synthesis (Ziaie et al. 2004) and biological applications (Holmes and Gawad 2010). The analysis mimics traditional bench-top laboratory performance in a miniaturized lab-on-a-chip (LOC) device, and it exhibits many advantages, such as reduced reagent consumption, rapid result readout, and multiplexed analysis (Novo et al. 2013). However, commercial deployment of microfluidics remains a challenge in many applications due to the requirement for a complex fluid handling system.

Pressure-driven flow microfluidics typically requires syringe pumps, tubing and other fluid interconnects and are often bulky and expensive which limits their portability (Pennathur 2008). Alternatives to pressure-driven flow have been motivated by the desire to miniaturize and simplify device designs for improved portability and decreased cost. Electrokinetic methods, such as electroosmotic flow which do not require an active pump, do require high voltages for transport (Stone et al. 2004). Although microfluidics has demonstrated a high potential in diagnostics, the practical limitations mentioned earlier have limited their deployment as commercial devices. When designing microfluidic sensors for resource-limited settings such as sub-Saharan Africa or remote portions of South

Electronic supplementary material The online version of this article (doi:10.1007/s10404-013-1317-3) contains supplementary material, which is available to authorized users.

F. He · S. R. Nugen (✉)
University of Massachusetts Amherst, Amherst, MA 01003, USA
e-mail: snugen@foodsci.umass.edu

America, additional considerations must be given (Yager et al. 2006, 2008). The ideal device must be easy to use, low-cost, and give rapid results.

Capillary flow is a good alternative to active pumping due to the lack of external pumps (Gervais et al. 2011). One of the most beneficial characteristics is the ability to transport liquids without the need for external pumps which simplifies the system and allows it to be further miniaturized. This simplicity is one of the reasons lateral flow assays, which incorporate capillary driving forces, are popular for diagnostics. The capillary flow within a microfluidic device is governed by several factors including the channel dimensions, liquid viscosity, and contact angle between the surface and solution. As most assay reagents are aqueous and polymeric substrates used for microfluidics are hydrophobic, reduction in the contact angle through surface modification has been an interesting area of research.

Modeling of the fluid flow in rectangular capillary channels has been proposed by Jong et al. (2007). They reported a final governing equation of:

$$t = \frac{6nL^2}{\rho g H h^2 + 2h\sigma cos\theta}$$

where t is time (s), n is the viscosity of the fluid (Pa s), L is the length of the flow at time t (m), ρ is the density of the fluid (kg/m^3), g is gravity (m/s^2), H is the height of the fluid in the inlet reservoir (m), h is the height of the channel (m), σ is the surface tension of the fluid (N/m), and θ is the contact angle between the fluid and surface (°). These modeling experiments were conducted in a hydrophobic channel using silicone oil as the media, and therefore, no surface modification was required. The above model provided a good fit to the experimental data.

Given these parameters, it is possible to manipulate fluid flow by altering the contact angle between a solution and microfluidic channel wall. Establishing domains of varying hydrophobicity within a microfluidic channel has previously been used to create a "time gate" where fluid flow rates slowdown in order to allow for an incubation period (Schulte et al. 2002). Varying hydrophobicity has also been used to create a mixer within a microfluidic channel (Swickrath et al. 2009). A surface coating is the most commonly used method to establish hydrophilicity such as the patterning of polyvinyl chloride with cellulose acetate to enable capillary flow (Swickrath et al. 2008).

Electrowetting (EW) is the phenomenon where the wettability of a surface can be altered with an applied potential. The surface consists of an electrode covered with a hydrophobic dielectric coating such as polytetrafluoroethylene (PTFE). When a potential is applied across the electrode, the surface hydrophobicity fluctuates to a lower contact angle. Electrowetting has been used for the discrete movement of liquid droplets across a plane as well as within a microfluidic channel (Pollack et al. 2002). Unfortunately, most microfluidic applications require significant voltages. Therefore, efforts have been made to decrease voltages by reducing the thickness of the dielectric layer (Saeki et al. 2001).

While this has been demonstrated using electrowetting on dielectric (EWOD) to manipulate the movement of droplets (Pollack et al. 2002; Saeki et al. 2001; Srinivasan et al. 2004), EWOD has also been used for microfluidic valves to control fluid flow (Mérian et al. 2012; Satoh et al. 2008). Satoh et al. (2008) demonstrated the valves in a PDMS channel over glass using sputter-coated gold electrodes. In this case, the contact angle was shifted from 72° to 25° following the voltage increase. The gold electrode contained a carbonaceous layer, resulting in the initial hydrophobicity. We have previously demonstrated the actuation of a valve with low voltage (Mérian et al. 2012). The thin hydrophobic layer required only a −0.9 V potential for the hydrophilicity shift. Mérian et al. used a fluorinated monolayer on a silver electrode to achieve an initial contact angle of ~148.1°. Following a 4.0 V potential, the contact angle was reduced to 21.9°. This valve was demonstrated in a single straight channel using 1 M KCl.

Although the final cost of a device is significantly influenced by the materials selected, the method of manufacture also must be considered. Ideally, low-cost devices would be manufactured in a continuous process with a high and efficient output. We are entering a new era of microfluidic biosensors which is seeing a focus shift to low-cost platforms such as paper fluidics and roll-to-roll manufacturing (Lee 2013). Roll-to-roll processing of LOC devices has been demonstrated to produce high-volume devices with a low cost (Liedert et al. 2012; Vig et al. 2011). Vig et al. constructed microfluidic separation devices on cellulose acetate film. The microchannels were thermally imprinted, and roll-to-roll lamination was used for device sealing. The team was able to produce 360 devices/h using the continuous method. A cost analysis of the device estimated each device to be 0.5 euros (approximately $0.66) for materials and manufacture.

Electrodes for microfluidic devices are commonly patterned using either photolithographic methods which involves the sputtering or evaporation of metals (Nugen et al. 2009), or screen printing where a conductive paste is patterned through a mesh (Noh et al. 2010). While photolithographic methods can offer exceptional feature sizes, the process is expensive and therefore not always applicable for high throughput, low-cost devices. Additionally, continuous fabrication of electronics using gravure coating of electrodes can be accomplished on a roll-to-roll manufacturing line (Noh et al. 2010). This method offers the

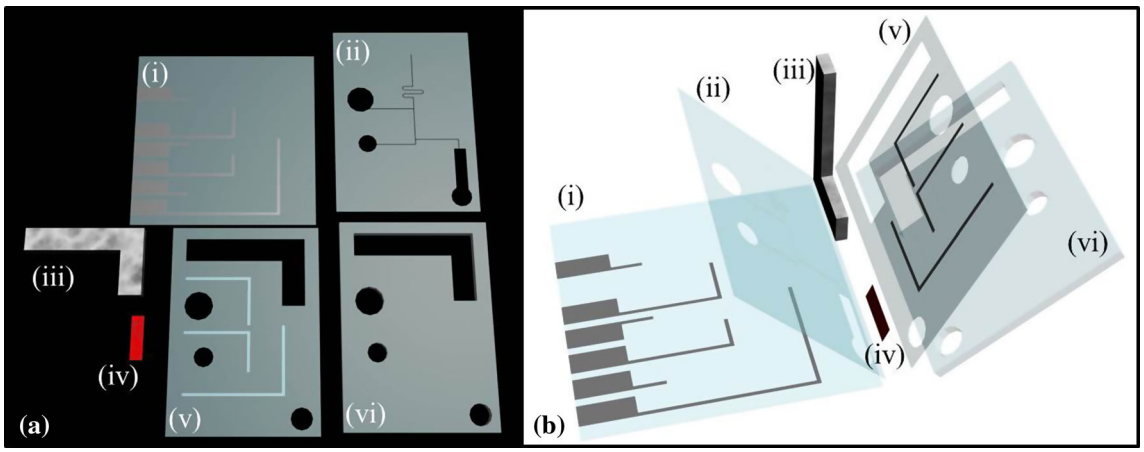

Fig. 1 Schematic representation of microfluidic device with three electrowetting valves. **a** the individual components of the microfluidic device consisted of (*i*) silver electrodes printed on PET. The electrodes were modified with a hydrophobic monolayer. (*ii*) A pressure-sensitive adhesive with laser-ablated channels. (*iii*) An absorbent pad for continued capillary flow. (*iv*) A conjugate pad containing dye. (*v*) Unmodified silver electrodes on PET. (*vi*) A PMMA layer to allow for a deeper sample well. **b** All layers were adhered together to enclose the microchannels

advantage of small feature sizes and low cost. Inkjet printing of electrodes offers the advantage of rapid prototyping and targeted patterning (Fukuda et al. 2013; Kwon et al. 2013; Lee et al. 2013; Perelaer and Schubert 2013; Ando and Baglio 2011). Inkjet printing has also been paired with roll-to-roll manufacturing for continuous processing (Perelaer and Schubert 2013).

In this paper, we introduced a low-cost, pump-free, capillary flow-driven microfluidic chip that can coordinate the flow of three reagents. The device is designed to allow future manufacturing using roll-to-roll assembly by incorporating flexible polymer films. We have additionally utilized inkjet printing for the low-cost patterning of electrodes. We have previously examined the chemical effects during this non-reversible electrowetting process and demonstrated a single electrowetting valve actuated PET-based microfluidic device (Mérian et al. 2012). We have designed and fabricated two prototypes of microfluidic devices. The first prototype contained a single electrowetting valve in a straight microchannel. Using this design, the effect of the applied voltage on the valve actuation times as well as the effect of the distance between the electrodes have been elucidated. Our second microfluidic device prototype contained three electrowetting valves for automating sequential fluid delivery.

2 Materials and methods

The first microfluidic prototype design was a single straight microchannel for characterization of the electrowetting valve. This device consisted of an 81-μm-pressure-sensitive-adhesive (PSA) tape (Adhesives Research, Glen Rock, PA), sandwiched between a 127 μm poly (ethylene terephthalate) (PET) film (3 M, St. Paul, MN) and a 1.6 mm rigid poly (methyl methacrylate) (PMMA) sheet (McMaster Carr, Santa Fe, CA). The second microfluidic device prototype consisted of laser-cut fluidic channels patterned in an 81-μm PSA tape and sandwiched between two 127-μm flexible PET films, a 1.6 mm PMMA sheet was put on top of the flexible chips to increase durability (Fig. 1). For both devices, prior to printing, the PET and PMMA were sonicated in 15 % 2-propanol, rinsed, and dried with nitrogen.

All patterns (channels and electrodes) were initially designed using AutoCAD (Autodesk, San Francisco, CA). The electrodes were printed onto both the PMMA and PET substrates using a Fuji Dimatix Inkjet Materials Printer (Dimatix DMP 2831, FujiFilm, Santa Clara, CA). A nanoparticle-free Ag-ink was used for printing the electrodes. The ink was synthesized using a procedure modified from previous reports (Walker and Lewis 2012). Briefly, 0.5 g of silver acetate was vortex mixed into 1.25 ml aqueous ammonium hydroxide at room temperature for 15 s. Formic acid (0.1 ml) was then titrated into the solution dropwise for 60 s (vortex mixing after each drop). The solution was undisturbed for 12 h and then filtered through a 220 nm syringe filter (Millipore Millex®, Billerica, MA). This clear solution, which contained 22 wt% silver, served as the reactive silver ink.

2.1 Laser cutting

A 40 W CO_2 laser system (Epilog Laser, Golden, CO, USA) was used to cut through the pressure-sensitive adhesive, PMMA, and PET film. In the first device model,

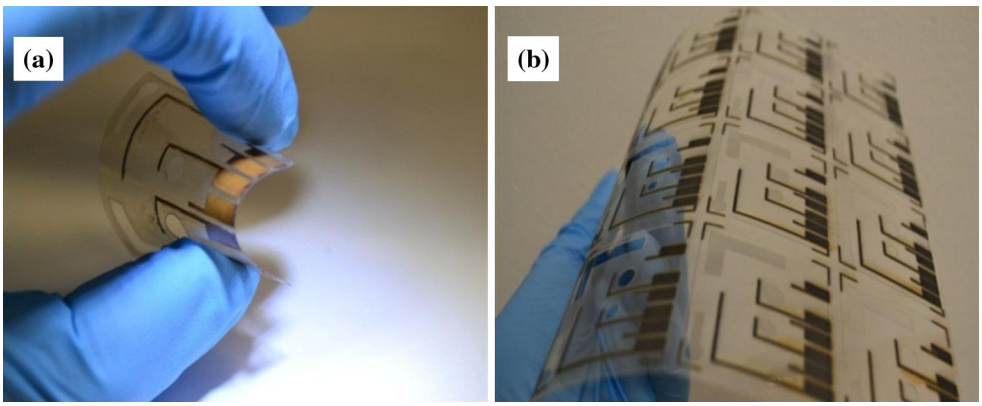

Fig. 2 **a** Flexible electrodes made by inkjet printing, **b** inkjet-printed Ag electrodes on a PET substrate film

the PMMA was cut with the laser in vector mode at 40 % speed, 25 % power; 5,000 Hz. The PET was cut with the laser in vector mode at 40 % speed, 5 % power; 5,000 Hz. For the pressure-sensitive adhesive, the film was cut in vector mode at 32 % speed, 5 % power; 5,000 Hz. A straight microchannel was laser ablated in the PMMA using vector mode at 40 % speed, 7 % power; 350 Hz, 500 focus. The off focus function of the laser system resulted to a height of about 230 μm of microchannel. In the second device model, the settings for cutting through PMMA, PET, and PSA tape remained the same as the first microfluidic model. For continuous flow, an absorbent pad (CF5, Whatman, England) was incorporated into the device. A 1-mm-deep cavity was laser ablated into the PMMA for the absorbent pad. For the absorbent pad cavity, the laser was used in raster mode with 30 % speed, 65 % power; 5,000 Hz.

2.2 Electrode printing

The electrodes were inkjet-printed onto the cleaned PET and PMMA surfaces using a 1 pL drop size. Prior to printing, both substrates were exposed to 7-min UV irradiation (254 nm, 30 mW/cm^2, Jelight Company, Inc., Irvine, CA). This treatment was performed to increase hydrophilicity of the polymer surface for improved printing quality. The temperatures of the printhead and plate stage were both set to 30 °C. The drop spacing of the pattern was set to 15 μm, which lead to a print resolution of 1,693 dpi. 10 % by volume of 2,3 butanediol was added into the reactive silver ink, which served as both a humectant and viscosifying aid (Walker and Lewis 2012). Ink droplets were produced using an ejection frequency of 2 kHz and a driving voltage of 40 V. A custom ejection waveform was generated in order to reduce satellite droplet formation and provide reliable inkjet printing. After printing, the electrodes were sintered at 90 °C for 1 h. Figure 2 shows the electrodes printed on the PET film.

2.3 Electrowetting valve characterization

The surface morphology of the inkjet-printed silver electrodes on PET substrate was observed by scanning electron microscope (SEM) (FEI Company, Hillsboro, OR). The height of the electrode was examined using a Zeta 20 3D optical profiler (Zeta Instruments, San Jose, CA) with bottom illumination and analyzed using Zeta 3D software (version 1.5).

To examine the relationship between the voltage needed to open the valve and the actuation time, a microfluidic chip (not shown) containing a straight microchannel and a single electrowetting valve were made. 1*H*,1*H*,2*H*,2*H*-Perfluorodecanethiol ($HS(CH_2)_2(CF_2)_7CF_3$, 97 %) was used to forma hydrophobic monolayer on the silver electrode (Sigma-Aldrich Corp., St. Louis, MO). A solution of 6 mM perfluorodecanethiol (PFDT) was prepared in deoxygenated absolute ethanol (200 proof). Modified Ag electrodes were made by manually pipetting 3 μl of the 6 mM PFDT solution directly on a 1 mm × 15 mm Ag electrode and to form a self-assembled monolayer (SAM). This device model included a transparent PMMA layer with a non-treated Ag electrode (1 mm × 15 mm), a double-sided PSA film containing a microfluidic channel as a middle layer, and another PMMA with PFDT modified Ag electrode (1 mm × 15 mm) as a bottom layer. The distance between two electrodes was 1, 3, or 6 mm separately.

In the second microfluidic device, modified Ag electrodes were made by immersing the bottom PET films into a 2 mM PFDT solution for 3 h to form the hydrophobic insulator, then rinsed with ethanol and DI water, and dried with nitrogen gas. Prior to bonding, top PET film was exposed to UV for 11 min, creating the hydrophilic surface for capillary fluid flow. A PMMA layer was adhered on top of this PET film to increase durability and allow for buffer inlet. As a result, microfluidic channels containing three electrowetting valves were fabricated. This microfluidic

device included a transparent PET film with inkjet-printed Ag electrodes as a bottom PET layer, a double-sided PSA film with a thickness of approximately 81 μm containing microfluidic channels as a middle layer, a top PET layer containing PFDT modified Ag electrode, and a PMMA layer contained an absorbent pad and a conjugate pad (Fig. 1).

2.4 Capillary flow requirements

In order to prevent capillary flow within the microfluidic channel, the hydrophobicity would have to be raised to a critical contact angle. The required contact angle was determined by the following formula (Jong et al. 2007):

$$t = \frac{6nL^2}{\rho g H h^2 + 2h\sigma cos\theta}$$

The dimensions of the microfluidic channel were inserted into the equation and the contact angle (θ) required for no within the channel ($t \geq 0$ for $L = 1$ mm). From this model, it was determined that a contact angle of >90° was required for flow to stop within the channel. Surfaces with a contact angle measurement less than this critical angle would result in a decreased velocity of the sample solution but not a complete stop. Therefore, the functionalized electrodes required a contact angle of >90° in order to result in a stop in fluid flow. It should be noted that given this model, a contact angle above 90° should always stop fluid flow due to a negative cos θ.

3 Results and discussion

3.1 Electrowetting valve characterization

Valve operation in the microfluidic device was evaluated visually by employing a conductive solution (1× PBS buffer, pH 7.4) mixed with 5 % blue food dye. Fluid moved uninhibited through the microchannel until reaching the modified Ag electrode. Once encountering the modified electrode valve, the capillary flow stopped. When the potential was applied, the flow continued past the modified electrode until it reached the end of the microfluidic channel. The time and voltage used to open the valve were also investigated quantitatively in the first microfluidic device. In addition, multiple electrowetting valve actuation was evaluated in the second microfluidic device containing three electrowetting valves (Fig. 5), visually, by employing three different conductive solution (1× PBS buffer, pH = 7.4) mixed with 5 % blue, yellow, and red food dye separately.

The electrode thickness was determined to be 54.9 ± 13.5 μm ($n = 3$) using optical profilometry. The

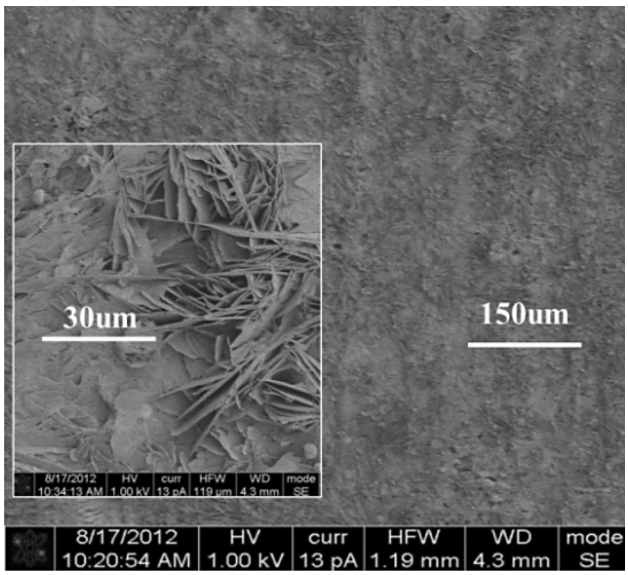

Fig. 3 Scanning electron microscopy (SEM) images of the surfaces of printed silver electrodes sintered at 90 °C for 30 min (prior to SAM monolayer modification)

surface morphology of the inkjet-printed silver electrodes (prior to monolayer modification) on PET substrate was analyzed by SEM (Fig. 3). The printed silver electrode sintered at 90 °C for 30 min presented an irregular surface. The inset, displaying higher magnification, showed irregular crystalline structures, which can be formed by evaporation of solvent in the ink, or entrapped air bubbles during sintering. The silver electrodes become conductive after sintering, indicating the formation of conductive path. The monolayer modified silver electrodes showed similar surface structure (Fig. 4).

Contact angle measurement was used for monolayer surface characterization. After modified by PFDT monolayer, the contact angle of the silver electrode was 162.3 ± 6.7° ($n = 3$), with full wetting following actuation. We have also quantified the surface chemistry of the silver electrodes using X-ray photoelectron spectroscopy (XPS) previously (Mérian et al. 2012). The surface chemical composition of PFDT modified silver electrode showed the presence of fluorine and sulfur which confirmed that the formation of a PFDT SAM was successful achieved. The results also showed that there were enhanced grafting of PFDT SAM following UV-treatment of the silver electrodes, due to increased hydrophilicity after UV-treatment.

Following deposition, the silver electrode contained well-defined crystalline structures as is shown in Fig. 4a. After the electrode was treated with the hydrophobic coating, the surface appeared physically damaged by the multiple washing steps as shown is shown in Fig. 4b. Additionally, the initial contact angle after monolayer modification showed significant variation (150.7 ± 8.0)

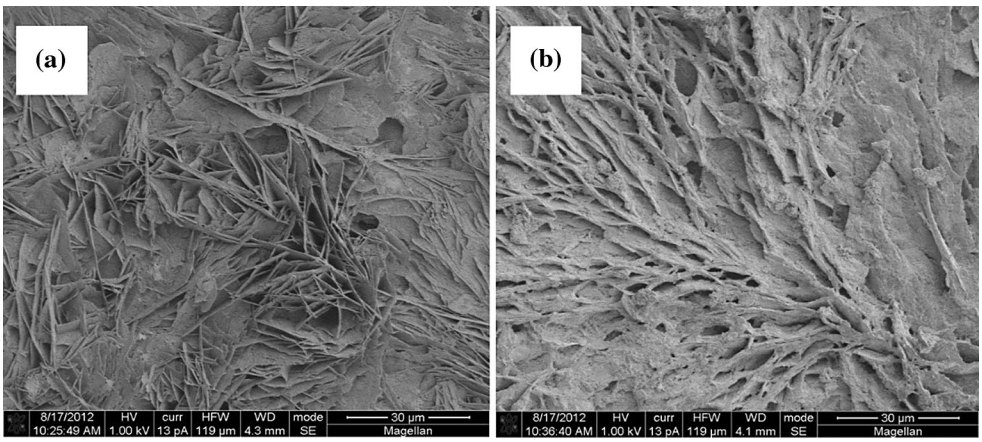

Fig. 4 Scanning electron microscopy (SEM) images of the surfaces of printed silver electrodes **a** prior to PFDT monolayer surface modification, **b** after PFDT monolayer surface modification. Both surface showed inconsistent surface roughness due to the ink solvent evaporation during the sintering process

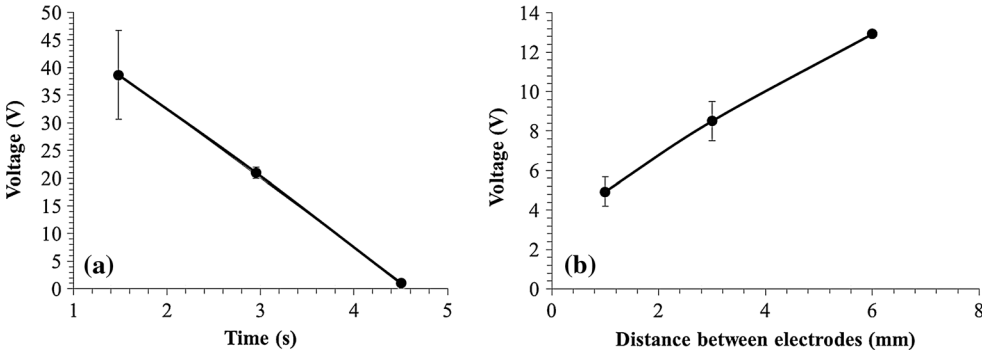

Fig. 5 **a** A dose response curve was constructed by integrating the voltage over time when the distance between two electrodes was 1 mm. The data represent a minimum of three replicates with the *error bars* representing the standard deviation. When no voltage was added, the hydrophobic electrode was able to stop the solution over 12 min. **b** A dose response curve was constructed by integrating the voltage over the distance between two electrodes. The voltage used to open the valve was able to actuate within 1 s. The data represent a minimum of three replicates with the *error bars* representing the standard deviation

due to the high variability of silver electrode surface roughness. While the high surface roughness allowed an overall hydrophobic surface, some surface characterization methods such as ellipsometry were difficult and therefore not reported.

In our EW experiment, we have used a 3 µl sessile droplet of electrolyte solution (1× PBS) for the electrowetting experiment, and the voltage was applied from 0 to 4 V. It was observed that at 2.0 V the contact angle change requires a longer actuation time (~2 min), but at 3 and 4 V the contact angle changes appreciably within a short time (~2 s). We have also performed EW experiment with a 3 µl sessile droplet of 1× PBS solution containing 5 % blue food dye. In these experiments, it was observed that at 3 V the contact angle also changed within 2 s. The change in contact angle with food dye was slightly larger (~17°) than the test with no food dye. We observed the phenomena in both tests that the apparent contact angle would reduce rapidly at a critical voltage (3.0 V). The critical voltage may represent the transition from the Cassie–Baxter to a Wenzel regime (Dai and Zhao 2008).

3.2 Fluidic timing

Using 1× PBS buffer (mixed with 5 % blue dye, pH 7.4) as a model solution, we measured the actuation time to open a closed valve as a function of the voltage and the distance between two electrodes in the valve, using a straight microchannel in PMMA chip. The results are shown in Fig. 5. The distance between two electrodes and was set to be 1, 3, and 6 mm, respectively. The time used to open the valve was found to increase when the distance between two electrodes increased, and the time was found to be decreased when the voltage added to open the valve increased. The results suggest that a voltage as low as 2.0 V was enough to actuate the valve, but increased

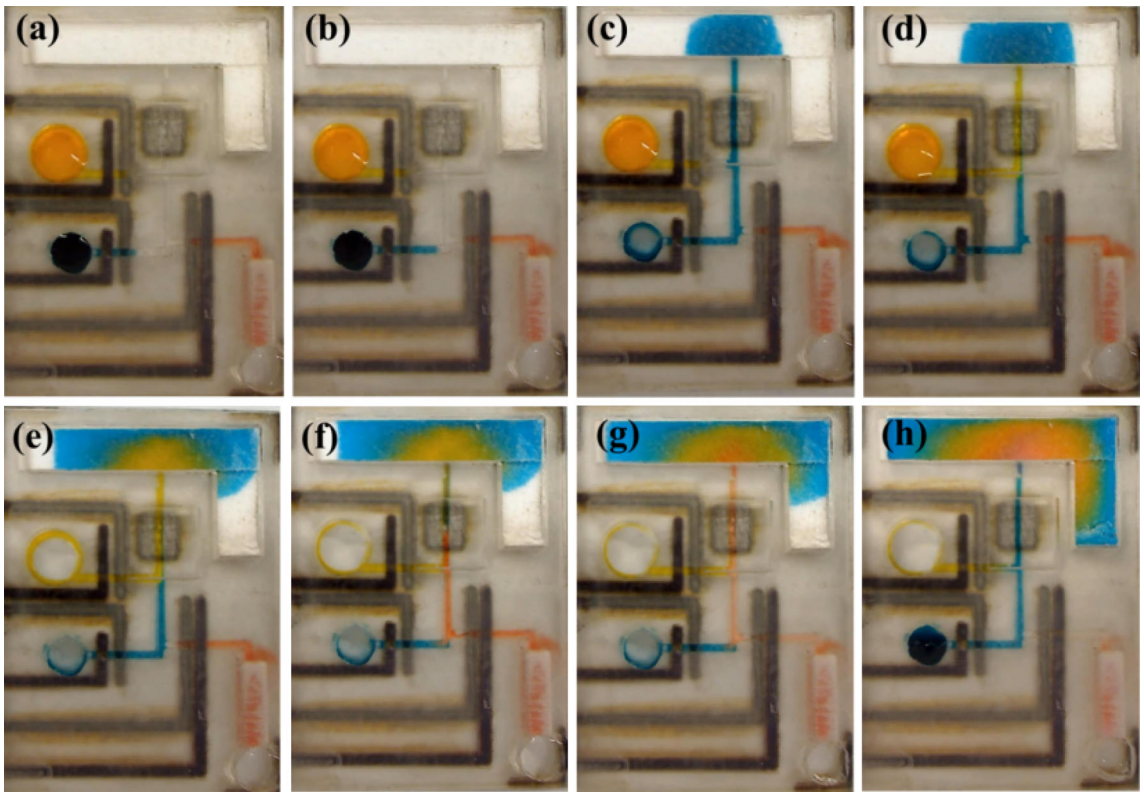

Fig. 6 The actuation of the multivalve. **a** A transparent PBS solution was added at the sample inlet; the *red* dye in the conjugate pad was released from the membrane and stopped at the valve. Two other solutions were added (1× PBS buffer with 5 % *yellow* and *blue* food dye) and stopped at the valves, **b** the valve for the *blue* solution was opened, **c** *blue* solution reached the absorbent pad by capillary flow, **d** the valve for the *yellow* solution was opened, **e** *yellow* solution reached the absorbent pad by capillary flow, **f** the valve for the *red* solution was opened, **g** *red* solution reached the absorbent pad by capillary flow, **h** Additional *blue* solution would not be stopped once the valve was opened. See video in supplemental materials (color figure online)

voltage resulted in a much more rapid response. Similarly, as expected, increasing the distance between electrodes required a larger voltage to actuate the valve within 1 s.

3.3 Automating device operation

Operations of normally closed electrowetting valves within a capillary driven microfluidic device were demonstrated, as shown in Fig. 6 and video S1. The valves were actuated using an eight-channel USB controlled relay connected to a computer. The timing of the valves could therefore be controlled programmatically. As expected, the dye solution was able to flow using capillary flow until reaching the hydrophobic electrode. It was demonstrated that the device was able to deliver the solutions sequentially to the absorbent pad.

Food dye was used as a visual aid in the valves actuation tests. The sequential delivery of the solutions could be seen in the absorbent pad which had a tiered color scheme following the experiment. We have showed that using food dye did not change the critical voltage because in both cases the contact angle changed rapidly at 3.0 V. And we observed no color change in the multiple valves actuation as is seen in Fig. 6. Therefore, we speculate that food dye did not has a significant effect on the critical voltage, and the impact of electrochemical degradation of food dye on electrowetting could be neglected during valve actuation, due to the short actuation time (<5 s) and low voltage (<5 V).

4 Conclusion

In this study, we have demonstrated *on-chip electrowetting valves* concept on a capillary polymeric microfluidic device. The device contained electrowetting valves for automating fluid delivery. The valves were fabricated by inkjet printing of reactive silver ink and modified with hydrophobic monolayer. The valves could be actuated at a low voltage (4 V), which allows for portable battery-powered devices (such as three 1.5 V AAA battery or watch batteries). The potential required to open the valve was applied to the electrode for a short time (<5 s), and therefore, the valve is relatively fast actuating.

Besides, the device was developed using low-cost materials. The size of the device could be miniaturized by using AAA batteries instead of a large power supply. The portability and low cost makes this device promising for point-of-care devices to be used in low resource settings. We believe that this technique will simplify the operation of microfluidic devices and could potentially allow for the performance of more complex assays in an autonomous fashion.

The ability to sequentially deliver solutions during in a capillary microfluidic device could significantly increase the complexity of assays low-cost tests. The power requirements on the chips are not significant and therefore would not require a larger controller. Future experiments could integrate a low-cost electrochemical reader with the control device to allow for transduction in a biosensor.

Acknowledgments This project was supported in part by the UMass Amherst Center for Hierarchical Manufacturing, a nanoscience shared facility funded by the National Science Foundation under NSF Grant #CMMI-1025020. The authors thank undergraduate researcher Elsa Zhao for her assistance with silver ink synthesis. The authors would also like to thank S. Brett Walker and Professor Jennifer A. Lewis for assistance with waveform of reactive silver ink.

References

Ando B, Baglio S (2011) Instrumentation notes inkjet-printed sensors: a useful approach for low cost, rapid prototyping. IEEE Instrum Meas Mag 14:36–40

Dai W, Zhao Y (2008) An electrowetting model for rough surfaces under low voltage. J Adhes Sci Technol 22:217–229

Fukuda K, Sekine T, Kumaki D, Tokito S (2013) Profile control of inkjet printed silver electrodes and their application to organic transistors. ACS Appl Mater Interfaces 5:3916–3920

Gervais L, Hitzbleck M, Delamarche E (2011) Capillary-driven multiparametric microfluidic chips for one-step immunoassays. Biosens Bioelectron 27:64–70

Holmes D, Gawad S (2010) The application of microfluidics in biology. In: Hughes MP, Hoettges KF (eds) Microengineering in Biotechnology. Humana Press, pp 55–80

Jong WR, Kuo TH, Ho SW, Chiu HH, Peng SH (2007) Flows in rectangular microchannels driven by capillary force and gravity. Int Commun Heat Mass Transf 34:186–196

Kwon O, Kim H, Ko H, Lee J, Lee B, Jung C, Choi J, Shin K (2013) Fabrication and characterization of inkjet-printed carbon nanotube electrode patterns on paper. Carbon 58:116–127

Lee A (2013) The third decade of microfluidics. Lab Chip 13:1660–1661

Lee Y, Kim S, Lee K, Myung NV, Choa Y (2013) Inkjet printed transparent conductive films using water-dispersible single-walled carbon nanotubes treated by UV/ozone irradiation. Thin Solid Films 536:160–165

Liedert R, Amundsen LK, Hokkanen A, Maki M, Aittakorpi A, Pakanen M, Scherer JR, Mathies RA, Kurkinen M, Uusitalo S, Hakalahti L, Nevanen TK, Siitari H, Soderlund H (2012) Disposable roll-to-roll hot embossed electrophoresis chip for detection of antibiotic resistance gene mecA in bacteria. Lab Chip 12:333–339

Mérian T, He F, Yan H, Chu D, Talbert JN, Goddard JM, Nugen SR (2012) Development and surface characterization of an electrowetting valve for capillary-driven microfluidics. Colloids Surf A Physicochem Eng Asp 414:251–258

Noh J, Yeom D, Lim C, Cha H, Han J, Kim J, Park Y, Subramanian V, Cho G (2010) Scalability of roll-to-roll gravure-printed electrodes on plastic foils. IEEE Trans Electron Packaging Manuf 33:275–283

Novo P, Volpetti F, Chu V, Conde JP (2013) Control of sequential fluid delivery in a fully autonomous capillary microfluidic device. Lab Chip 13:641–645

Nugen SR, Asiello PJ, Connelly JT, Baeumner AJ (2009) PMMA biosensor for nucleic acids with integrated mixer and electrochemical detection. Biosens Bioelectron 24:2428–2433

Pennathur S (2008) Flow control in microfluidics: are the workhorse flows adequate? Lab Chip 8:383–387

Perelaer J, Schubert US (2013) Novel approaches for low temperature sintering of inkjet-printed inorganic nanoparticles for roll-to-roll (R2R) applications. J Mater Res 28:564–573

Pollack M, Shenderov A, Fair R (2002) Electrowetting-based actuation of droplets for integrated microfluidics. Lab Chip 2:96–101

Rivet C, Lee H, Hirsch A, Hamilton S, Lu H (2011) Microfluidics for medical diagnostics and biosensors. Chem Eng Sci 66:1490–1507

Saeki F, Baum J, Moon H, Yoon JY, Kim CJ, Garrell RL (2001) Electrowetting on dielectrics: reducing voltage requirements for microfluidics. Abstr Pap Am Chem Soc 222:8-PMSE

Satoh W, Yokomaku H, Hosono H, Ohnishi N, Suzuki H (2008) Electrowetting-based valve for the control of the capillary flow. J Appl Phys 103:034903

Schulte TH, Bardell RL, Weigl BH (2002) Microfluidic technologies in clinical diagnostics. Clin Chim Acta 321:1–10

Srinivasan V, Pamula VK, Fair RB (2004) An integrated digital microfluidic lab-on-a-chip for clinical diagnostics on human physiological fluids. Lab Chip 4:310–315

Stone HA, Stroock AD, Ajdari A (2004) Engineering flows in small devices: microfluidics toward a lab-on-a-chip. Annu Rev Fluid Mech 36:381–411

Swickrath MJ, Shenoy S, Mann Jr JA, Belcher J, Kovar R, Wnek GE (2008) The design and fabrication of autonomous polymer-based surface tension-confined microfluidic platforms. Microfluid Nanofluid 4:601–611

Swickrath MJ, Burns SD, Wnek GE (2009) Modulating passive micromixing in 2-D microfluidic devices via discontinuities in surface energy. Sens Actuators B Chem 140:656–662

Vig AL, Makela T, Majander P, Lambertini V, Ahopelto J, Kristensen A (2011) Roll-to-roll fabricated lab-on-a-chip devices. J Micromech Microeng 21:035006

Walker SB, Lewis JA (2012) Reactive silver inks for patterning high-conductivity features at mild temperatures. J Am Chem Soc 134:1419–1421

Yager P, Edwards T, Fu E, Helton K, Nelson K, Tam MR, Weigl BH (2006) Microfluidic diagnostic technologies for global public health. Nature 442:412–418

Yager P, Domingo GJ, Gerdes J (2008) Point-of-care diagnostics for global health. Annu Rev Biomed Eng 10:107–144

Ziaie B, Baldi A, Lei M, Gu Y, Siegel R (2004) Hard and soft micromachining for BioMEMS: review of techniques and examples of applications in microfluidics and drug delivery. Adv Drug Deliv Rev 56:145–172